recovery energy environment economy
2011 CSPG CSEG CWLS Convention

S-wave Attenuation within the Weathering Layer of an Alberta Heavy Oil Field

Kristof De Meersman
CGGVeritas, Calgary, Canada
kristof.DeMeersman@cggveritas.com

Summary

This work uses data from a permanent monitoring 3D 3C seismic experiment at the Peace River heavy oil field in Alberta, Canada, to quantify S-wave seismic attenuation (Q) in the top 12 meters of overburden. Q values are measured from the spectral ratios of up-going and down-going S-wave refraction energy at each receiver. These up-going and down-going wave fields are estimated from raw vertical and radial component data. Most Q values range between 8 and 22 with a median value of 13.5. A general North-South trend is observed with lower Q values (more S-wave attenuation) in the North where muskeg-type soils dominate.

Introduction

In 2009, CGGVeritas and Shell conducted a joint 4D monitoring experiment at the Peace River heavy oil field, using 482 buried 3C receivers and 11 buried and continuously emitting mini-vibrator sources. The sources and receivers were installed at typical depths of 80 m and 12 m respectively. The nominal receiver interval is 20 m with an 80 m receiver line interval (Forgues and Schisselé, 2010). Data that was recorded continuously over 84 days was averaged to produce a single dataset for use in this study. Even though the primary objective of this experiment was 4D reservoir monitoring we show that the acquisition system and survey design are ideally suited to obtain estimates of S-wave attenuation for the top soil. Low S-wave velocities (large statics) and high absorption rates (low Q) within the weathering layer are considered to be primary causes for the reduced bandwidth and signal-to-noise of converted-wave (PS) data when compared to conventional P-wave (PP) data (Bale and Stewart, 2002).

Method

The idea to measure near-surface attenuation using buried three-component receivers stems from the observation that such arrays measure the wave field at two instances. Any seismic energy that is reflected, refracted or generated at a depth below the buried receiver array is recorded first as it passes through the array while propagating towards the earth's surface. This up-going primary energy is then reflected down at the free surface and recorded a second time as it propagates back down into the earth. This later, secondary arrival consists of down-going, or ghost energy. In principle, it should be possible to estimate an effective measure of Q for the soil layer between the surface and the buried array by applying the log-spectral ratio method on the primary and ghost wave fields. Before Q can be estimated it is however important that we understand the nature and kinematics of the recorded S-waves as well as develop a method for separating them into their up-going and down–going parts.

The seismic source used in this experiment is in essence a dipole with a long axis that is oriented in the vertical direction. Dipole sources are highly directional and emit both P-waves and S-waves (Figure 1). The theoretical radiation pattern is rotationally symmetric about the vertical. Maximum P-wave energy is emitted vertically while none is emitted horizontally. Maximum S-wave energy is emitted at a 45^{o} angle

from vertical in both the upwards and downwards directions. A representative vertical and radial component shot gather is shown in Figure 2. Both components show abundant coherent P-wave reflections as well as some coherent 'first break' S-wave arrivals that are followed mainly by scattered S-wave noise. The lack of clear S-wave reflections is a consequence of the source not emitting S-wave energy vertically. The coherent first break S-wave event consists of two distinct arrivals (Figure 1). The first is the direct arrival from upwards emitted S-wave energy. The second is a refraction generated by the downwards emitted S-waves. Most of this energy is emitted at 45° and we expect this to reach critical angles at relatively limited offset and depth from the source.

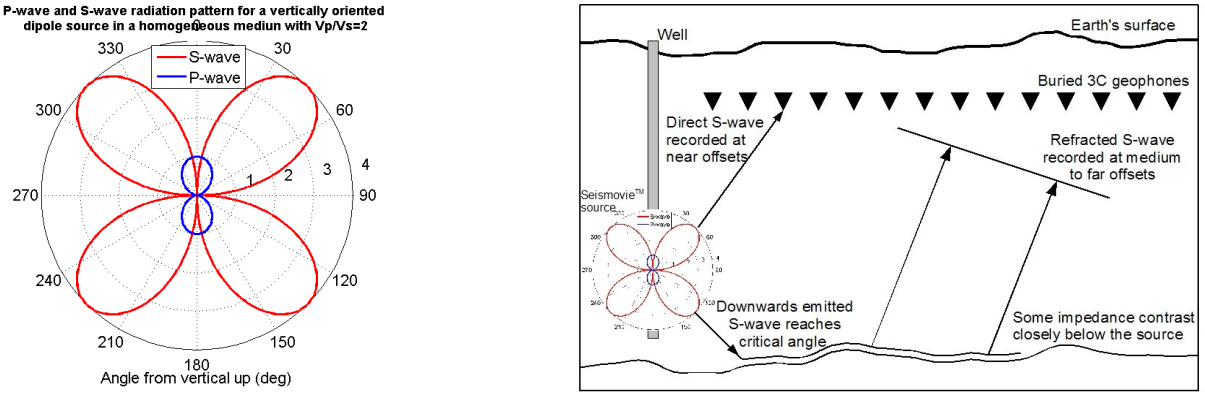

Figure 1: (left) Theoretical radiation pattern for P-wave and S-wave energy for a vertically oriented dipole source (moment tensor with nonzero 33 couple) in a homogeneous medium with V_P/V_S =2 (Aki and Richards, 2002). (Right) The origin of the two dominant S-wave arrivals that can be observed on the field data in Figure 2.

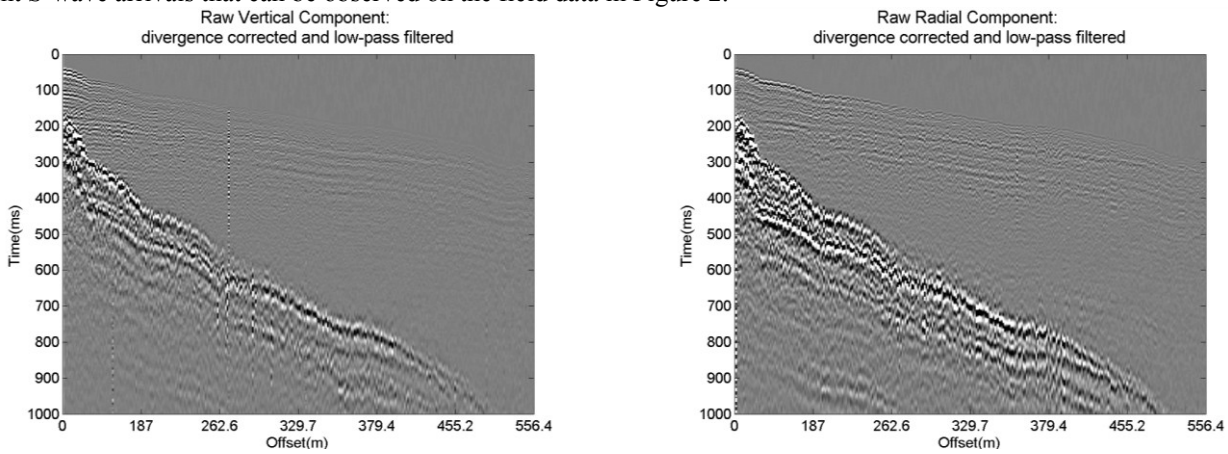

Figure 2: Example of a typical vertical and radial component shot gather.

One useful property regarding refractions in general is that they reach the receivers at a common propagation angle (i.e. as a plane wave). This is true for receivers that are at a common depth within a 1D velocity structure. We will also assume that the bulk of the refracted energy in our experiment can be explained in terms of a single refracting layer and hence a single, unique ray angle at the recording level. Under these assumptions the recorded S-wave refraction energy on the vertical (**V**) and radial (**R**) components of the buried array can be written in terms of a primary energy (**P**), ghost energy (**G**) and a ray angle θ and measured from vertical:

$$\begin{bmatrix} \mathbf{V} \\ \mathbf{R} \end{bmatrix} = \begin{bmatrix} -\sin(\theta) & \sin(\theta) \\ \cos(\theta) & \cos(\theta) \end{bmatrix} \begin{bmatrix} \mathbf{P} \\ \mathbf{G} \end{bmatrix} \Leftrightarrow \mathbf{d} = \mathbf{Am} \qquad (1)$$

Up-down separation of the refracted S-wave can be achieved by inverting **A**, yielding the true-amplitude expressions for the up-going and down-going refracted S-wave shown below. A grid search provided an optimal ray angle for separation of θ=30° with the resulting data shown in Figure 3.

$$\begin{bmatrix}\mathbf{P}\\ \mathbf{G}\end{bmatrix}=\frac{1}{\sin(2\theta)}\begin{bmatrix}-\cos(\theta) & \sin(\theta)\\ \cos(\theta) & \sin(\theta)\end{bmatrix}\begin{bmatrix}\mathbf{V}\\ \mathbf{R}\end{bmatrix} \qquad (2)$$

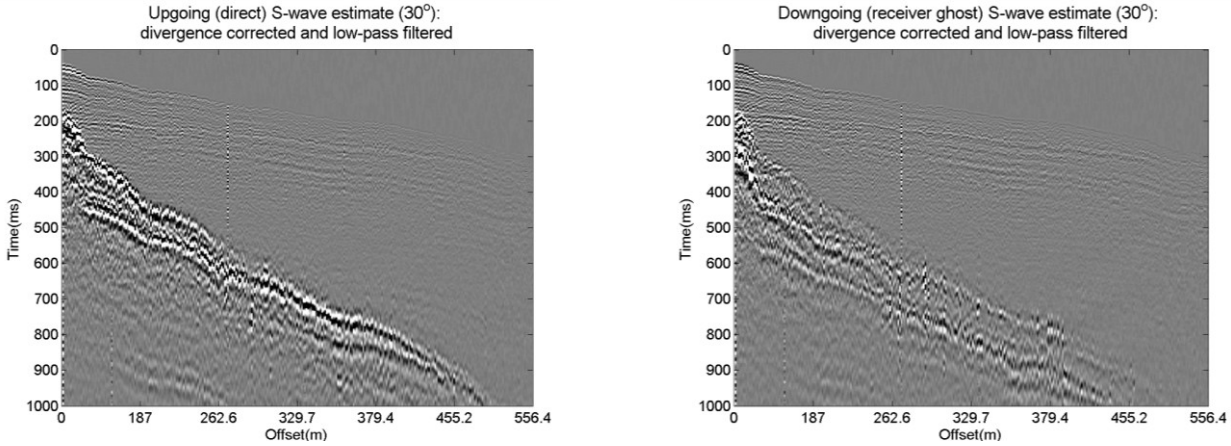

Figure 3: Data from Figure 2 after separation into Primary and Ghost components using equation 2 and a ray angle of 30°. The Primary and Ghost estimates are shown in true relative amplitude.

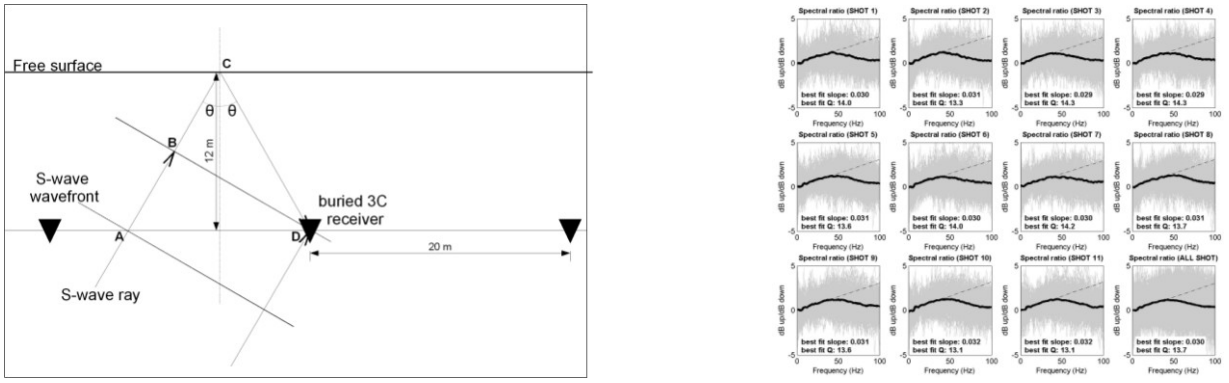

Figure 4: (Left) Geometrical relationship between primary and ghost arrivals as measured by the buried receivers. (Right) Log spectral ratio curves between primary and ghost spectra from all receivers and shots. The black lines represent the average spectral ratio for each shot and the dashed lines represent the L1-norm gradient fitted for frequencies between 5 and 45 Hz.

Q values are estimated using a log-spectral ratio approach that was adapted to the geometry of this experiment (Figure 4). We define $Q=\frac{\pi}{\gamma}\frac{\Delta t}{\cos^2(\theta)}$. The gradient of the log-spectral ratio between the primary and ghost S-wave is given by γ and the arrival time difference between them is given by Δt. Both properties are measured at the same receiver. Ideally, one would compute the gradient γ of the log spectral ratio between the up-going S-wave energy at A and the down-going energy at D. These locations represent the same point on the wave front at different times. No receiver is located at A, but the distance between A and D is small (≈14 m). Therefore, the up-going amplitude at D can be used to substitute for that at A. One important advantage of taking ratios of spectra form the primary and ghost at the same receiver location is that this will yield Q values that are not biased by coupling variations between the different receivers. Our γ-values are obtained by L1-fitting a straight line through the origin for spectral ratio, therefore assuming a free surface reflection coefficient of -1 and neglecting amplitude spreading (Figure 4). The Δt values relate to the travel path |BC|+|CD| in Figure 4. The $\cos^2(\theta)$ term in our definition for Q scales the Δt-value so that it relates to the travel path |AC| to |CD| over which γ is computed. Cross-correlating the primary and ghost arrivals for all stations yielded an average Δt-value of 100 ms for this survey and θ=30°.

Results

A map of Q values as well as a lidar image of the survey area is shown in Figure 5. The Q map was obtained after applying spatial averaging on the 11-shot median Q value for each receiver. Most Q values range between 8 and 22 with a median value of 13.5. There appears to be a general North-South trend with lower Q values and therefore more S-wave attenuation to the North. The lidar image was used to determine the boundary of the muskeg (swamp) in the surveyed area. The image confirms that Lower Q values are –in general- associated with muskeg soils. The muskeg has Q values in the range of 10 while parkland to the south has typical Q values of 15 and higher.

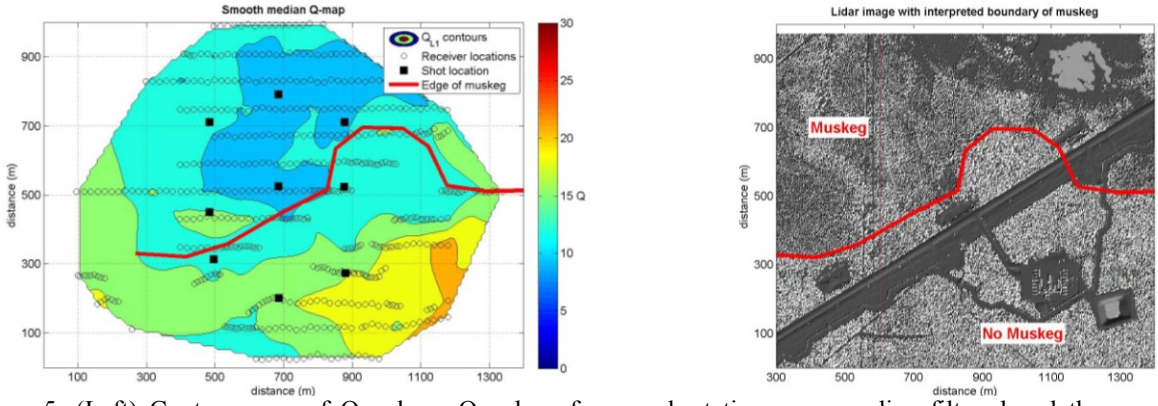

Figure 5: (Left) Contour map of Q values. Q values from each station were median filtered and then smoothened prior to contouring. (Right) Lidar image with the red line showing the interpreted edge of muskeg, or swamp soils (red line). This red line is also transferred to the Q contour map on the left.

Conclusions

This work uses data from a permanent monitoring 3C seismic experiment at the Peace River heavy oil field to quantify S-wave seismic attenuation (Q) for the top 12 meters of overburden. The Q values are measured at each 3C receiver location from the spectral ratios of up-going and down-going S-wave refraction energy. We present a method to estimate these up-going and down-going wave fields from raw vertical and radial component field data. The Q values range between 8 and 22, with a median value of 13.5. Lower Q values are typically associated with muskeg. This work is valuable in that it quantifies S-wave attenuation within the weathering layer of a heavy oil field with high spatial resolution. Moreover, it could lead the way to more deterministic Q compensation. Given the generally low S-wave Q values this is especially valuable in the processing of converted wave data where near surface Q can significantly impact overall signal-to-noise, statics, resolution etc.

Acknowledgements

The author would like to thank Shell and CGGVeritas for their kind permission to present this work and Michael Kiehn (Shell) for contributing the lidar image. Many thanks also go to Bruce Mattocks.

References

Aki, K. and Richards, P.G. [2002]. Quantitative Seismology, Second Edition, University Science Books, Sausalito, California.

Bale, R. and Stewart, R. [2002] The impact of attenuation on the resolution of multicomponent seismic data, 72nd Annual International Meeting of the Society of exploration Geophysicists, Expanded Abstracts, 1034-1037.

Forgues, E. and Schisselé E. [2010]. Benefits of Hydrophones for Land seismic Monitoring., 72nd EAGE Conference and Exhibition, Expanded Abstracts, B034

Tonn, R. [1991] The determination of seismic quality factor Q from VSP data: A comparison of different computational methods. Geophysical Prospecting, 39, 1-27.